Extended Focused Imaging in a Holographic Microscopy Imaging System

Zhenbo Ren, Ni Chen, Antony C. S. Chan, Edmund Y. Lam*
Imaging Systems Laboratory, Department of Electrical and Electronic Engineering,
The University of Hong Kong, Pokfulam, Hong Kong
*Email: elam@eee.hku.hk

***Abstract*—In most optical imaging systems, a three-dimensional object lying within the depth-of-field (DOF) will produce a clear and sharp image, while the parts outside will become blurry. Therefore, especially in microscopy, increasing the DOF is highly desirable, which can be achieved computationally through extended focused imaging (EFI). To construct the EFI image, we first use a depth-from-focus algorithm to create a depth map for each pixel by calculating its entropy. Based on the depth map, we show how to achieve EFI in a holographic microscopy imaging system called optical scanning holography. Computational results on objects with multiple axial sections are presented to validate the proposed approach.**

I. Introduction

Since the invention of holography in 1948 [1], this imaging technique has been used for recording and reconstructing real-world three-dimensional (3D) objects due to its full-parallax property. With charge-coupled devices (CCDs), hologram can be recorded and stored digitally as an interference pattern in a computer. This kind of holographic imaging technique is termed digital holography. There are many forms of digital holography, but the present work is concerned with a particular form called optical scanning holography (OSH) [2], which has the distinctive ability to image fluorescent specimens [3], making it particularly suitable for biological microscopy applications [4].

Typically in OSH, the volume information of a 3D object which contains several sections in space is digitally recorded with an active 2D lateral scanning procedure on a CCD. Reconstruction can be done numerically to obtain the object's sectional information. However, when one specific section is reconstructed, other sections will manifest as defocus noise appearing in the reconstructed image. The crosstalk introduced by other sections becomes worse when more sections are contained in the object. One solution to handle this problem is to suppress the defocus noise so that the slice we are focusing on is clear and sharp. Wiener filter [5], Wigner distribution function [6] and inverse imaging approach [7], [8], [9] have been proposed to recover sectional information within the depth-of-field (DOF). However, in some applications such as microscopy, we should not discard information on other sections. The whole scene of what we have captured should be clear enough for visualization and further analysis. Besides, the DOF of a microscope is usually not sufficient to obtain a single image in which every section of the object is in focus. Consequently, creating a single image where different sections locating at different positions along the longitudinal axis are brought to focus, is a challenging but important task.

To address this problem, which is to obtain the extended focused imaging (EFI) of a 3D object, and which is also called extended depth-of-field (EDOF), two major approaches have been proposed. The first is based on a specially designed phase plate, which is termed wavefront coding. In the optical path of a microscope, such a phase plate will facilitate an extension of the DOF of the images observed and magnified by the microscope [10], [11], [12]. The alternative solution constructs a single EFI image from a series of images obtained by scanning the 3D object on different sections mechanically, which is also called focus stacking [13], [14]. However, both approaches have drawbacks. For the former, a specially-designed phase plate has to be fabricated and put along the optical path of the imaging system. Apart from the expected phase shifting, undesired aberration in optics and adjustment for optical path increase the complexity experimentally. The second solution synthesizes an EFI image by using montage. To acquire a stack of images in which each section is focused one by one for montage, multiple scanning steps and precise movements and calibrations for each single image acquisition pose severe limitations on acquiring the collection of partially in-focus images, consequently confining the application of this method [15], [16], [17]. Besides, computational photography techniques such as light field imaging [18], coded aperture [19] and image fusion [20], [21] have also been used to extend the DOF.

In this paper, we present a numerical approach for constructing the EFI from a collection of digital holographic reconstructions in OSH. First we create a depth map by using a depth-from-focus (DFF) algorithm, which recovers depth information by computing a focus measure based on entropy for each pixel. We then combine the depth map and the reconstructions from the hologram to construct the EFI. Section 2 describes the recording and reconstruction processes of OSH and our experimental setup. In Section 3, we introduce focus detection for OSH. The algorithm for computing the depth map using DFF approach is also discussed. Section 4 presents the simulation results of constructing EFIs for a two-section object and a three-section object in OSH respectively. In Section 5 we draw the conclusion about our proposed approach and discuss the benefits and limitations of the EFI algorithm.

II. Optical Scanning Holography

In OSH imaging system, a 3D object is scanned by an active scanner with a complex-valued Fresnel-zone-plate (FZP) impulse response. The diffracted and scattered light through

978-1-4799-8633-0/15/$31.00 ©2015 IEEE

the object is collected with a single-pixel CCD detector. Heterodyne detection is employed to demodulate the real part and imaginary part of the electronic hologram. In our set-up, this demodulation is done numerically [7]. Thus a complex hologram containing 3D position information of the diffracted propagation through the object is recorded. The optical set-up of OSH imaging system in our laboratory is shown in Fig. 1(a). In optics, we generally model a 3D object as multiple sections discretely distributed in space. In this paper, the experimental 3D object is composed of either two sections "H" and "K", or three sections "H", "K" and "U". Fig. 1(b) and Fig. 1(c) show these two cases.

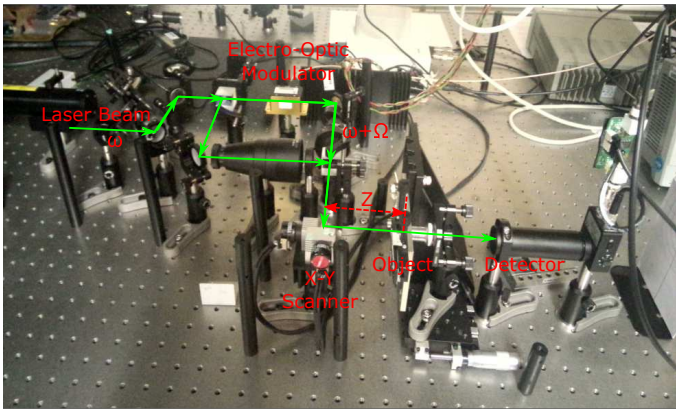

(a)

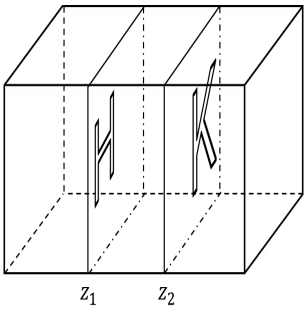

(b)

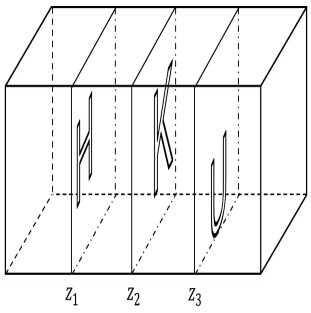

(c)

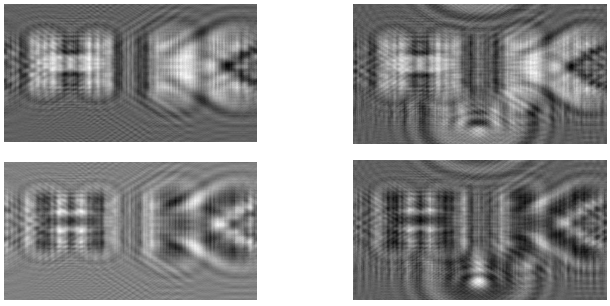

(d)

(e)

Fig. 1. (a) Optical set-up of OSH system. ω and Ω are initial carrier frequency of laser and shifted frequency respectively, z is the distance between the object and scanner. (b) Object with two sections "H" and "K" at z_1 = 10 mm and z_2 = 20 mm respectively. (c) Object with three sections "H", "K" and "U" at z_1 = 10 mm, z_2 = 15 mm and z_3 = 20 mm respectively. (d) Real part (above) and imaginary part (bottom) of hologram of (b). (e) Real part (above) and imaginary part (bottom) of hologram of (c).

As stated above, with our OSH imaging system, a 3D object can be recorded as a hologram. Fig. 1(d) and Fig. 1(e) present two holograms of the two-sectional object and three-sectional object. Mathematically, assuming the 3D object is expressed as $\sum_{i=1}^{k} o(x,y;z_i)$, where k is the total number of sections, (x,y) is the spatial coordinate, and z is the distance where each section is located. Then the hologram $g(x,y)$ can be computed as $g(x,y) = \sum_{i=1}^{k} |o(x,y;z_i)|^2 * h(x,y;z_i)$, where $*$ denotes 2D convolution, and $h(x,y;z_i)$ means the corresponding FZP at z_i. In our cases, $k=2$ and $k=3$ stand for two-sectional and three-sectional objects respectively.

In conventional reconstruction, to reconstruct individual section, we need to deconvolve the hologram $g(x,y)$ with conjugate FZP, which is $h^*(x,y;z)$. For instance, if the section "H" is to be reconstructed in two-section case, we need to know the distance parameter z_1 to create $h^*(x,y;z_1)$. Experimentally the distance between a particular section and the scanner is unknown. This process is related to focus detection.

Mathematically, the reconstructed image $r(x,y;z_1)$ of section "H" can be represented as [7]

$$\begin{aligned} r(x,y;z_1) &= g(x,y) * h^*(x,y;z_1) \\ &= \left[\sum_{i=1}^{k=2} \left|o(x,y;z_i)\right|^2 * h(x,y;z_i)\right] * h^*(x,y;z_1) \\ &= \Big[\left|o(x,y;z_1)\right|^2 * h(x,y;z_1) + \left|o(x,y;z_2)\right|^2 \\ &\quad * h(x,y;z_2)\Big] * h^*(x,y;z_1) \\ &= \left|o(x,y;z_1)\right|^2 + \left|o(x,y;z_2)\right|^2 \\ &\quad * h(x,y;z_2 - z_1), \end{aligned} \tag{1}$$

where $h(x,y;z_2-z_1) = h(x,y;z_2) * h^*(x,y;z_1)$. Since the hologram $g(x,y)$ and the FZP $h(x,y;z)$ are complex, the reconstruction $r(x,y;z)$ is also complex. Generally we display the magnitude of a complex reconstruction.

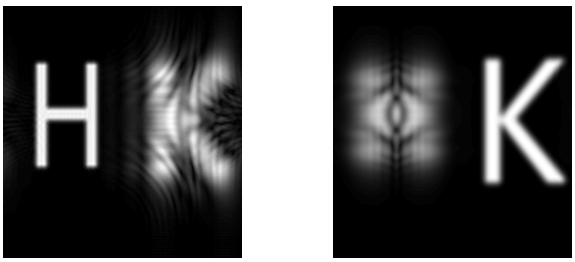

(a) (b)

Fig. 2. (a) Reconstructed image at z_1 = 10 mm. (b) Reconstructed image at z_2 = 20 mm.

In Eq. 1, the second term $|o(x,y;z_2)|^2 * h(x,y;z_2-z_1)$ acts as defocus noise which makes the reconstruction blurry. As the reconstructed images in Fig. 2 show, the targeting section is sharp, whereas the other section results in defocus noise which severely affects the post-analysis of the structure of the 3D object. Therefore it is necessary to construct one

single reconstructed image in which every section is sharp and defocus noise is suppressed.

III. Focus Detection and Extended Focused Imaging

For an imaging system, the DOF is usually limited. Within the DOF, objects show acceptable sharpness in the acquired image, which decreases gradually on each side of the focused distance of the lens. DOF is influenced by several factors, such as focal length of the lens, distance between lens and object etc. Hence it is essential to detect the focal length in order to reconstruct a sharp image [22]. In recent years, different methods are proposed to find the focal distance within a scene. Focus measures such as variance [23], [24], correlation [25], and gradient [26] are applied to situations such as macroscopic 3D object recording. Fresnelet bases [27], spectral ℓ_1 norms [28], and Wigner distribution [29] are proposed in a more mathematical way. Besides, computational imaging techniques such as changing camera aperture [30], [31], [32] and estimating depth from image structure or defocus [33], [34], [35] have also been proposed. In our proposed approach, focus detection is based on entropy minimization. We proceed to illustrate how to estimate the best depth for each pixel in reconstruction with the help of entropy.

A. Focus Detection

Entropy is normally used to measure how much information a transmitted message includes. In image processing, entropy is a measure of sharpness of an image. The sharper an image is, the more high frequency it includes, then the smaller the entropy is [36]. In this paper, for an $M \times N$ pixels image, Shannon entropy is computed as

$$e = -\sum_{x=1}^{M}\sum_{y=1}^{N} \frac{|R(x,y)|^2}{P} \ln \frac{|R(x,y)|^2}{P}, \tag{2}$$

where, $R(x,y) = \mathrm{Re}\{r(x,y)\}$ is the real part of the complex reconstruction $r(x,y)$, $P = \sum_{x=1}^{M}\sum_{y=1}^{N} |R(x,y)|^2$ is the total power of an image, e is the entropy of this image.

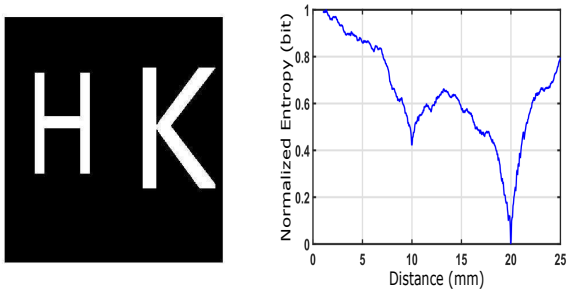

(a) (b)

Fig. 3. (a) Projection of 3D object with two sections "H" and "K" at z_1 = 10 mm and z_2 = 20 mm respectively. (b) Focus detection based on entropy.

Fig. 3 presents an example of detecting focus with entropy minimization. Fig. 3(a) shows the projection of two sections discretely distributed in space. Focus detection aims to determine the exact distances of each section. First, the hologram is reconstructed along z-axis in a range of $[1, 25]$ mm. For each reconstruction, we compute the entropy for the real part, and thus we have an entropy curve shown in Fig. 3(b). The horizontal axis is reconstruction distance with unit mm, and the vertical axis is normalized entropy with unit bit. Then for this case, two local minimum points arrive at z_1 = 10 mm and z_2 = 20 mm. Therefore we can assert that two separate sections are located at different depth in 3D space. Based on this principle, we determine the best in-focus distance of every pixel in constructing the EFI image later.

B. Depth-From-Focus and Extended Focused Imaging

As discussed above, we want to create an EFI image in which each section is in focus. While for each individual section along z-axis, the in-focus position varies. Therefore, if we gather together all pixel values which come from their in-focus reconstructions in one single image, this image should be the EFI image. In other words, if every pixel in one image is in focus, each section should also be in focus with a sharp reconstruction. Therefore we need to determine the best in-focus position for each pixel.

In reconstruction, the hologram $g(x,y)$ is reconstructed along z-axis from $z_1, z_2, \ldots,$ to z_k, altogether k reconstructions. The searching range $[z_1, z_k]$ should be determined according to the possible structure of the 3D object recorded in the experiment. Since when the 3D object is set up in the optical path, we can estimate a preliminary range of search in which the object is located. By stacking all the reconstructed images together, we have a volume of reconstructions $r(x,y,z)$, where $z \in [z_1, z_k]$. $r(x,y,z)$ is a 3D matrix with a size of $M \times N \times k$, and the real part of this volume of reconstructions is $R(x,y,z)$. We search the in-focus position for each pixel based on entropy minimization.

Since the entropy of an image is computed based on a 2D image. Therefore, to compute the entropy for a particular pixel, we need to use a block with a specified size to filter out the pixel and its adjacent pixels. We assume the block size is $t \times t$, in which t should be odd to guarantee the targeting pixel is located at the center of the block. We can define a 3D matrix $E(x,y,z)$ as the entropy map to store 2D entropy maps at each reconstruction distance. For any pixel (u,v), where $u = 1, 2, \ldots, M$, $v = 1, 2, \ldots, N$, the entropy in each overlapping block at the i-th reconstruction depth z_i is computed with

$$E(u,v,z_i) = -\sum_{x=u-\hat{t}}^{u+\hat{t}}\sum_{y=v-\hat{t}}^{v+\hat{t}} \frac{|R(x,y,z_i)|^2}{P} \ln \frac{|R(x,y,z_i)|^2}{P}, \tag{3}$$

where $\hat{t} = \frac{t-1}{2}$.

For the reconstruction $R(x,y,z_i)$ at the i-th reconstruction depth z_i, $M \times N$ entropies of $M \times N$ pixels are computed according to Eq. 3. For other reconstruction distances, the computing procedure is the same. After calculating all distances from z_1 to z_k, we can acquire the 3D matrix $E(x,y,z)$ storing k 2D entropy maps.

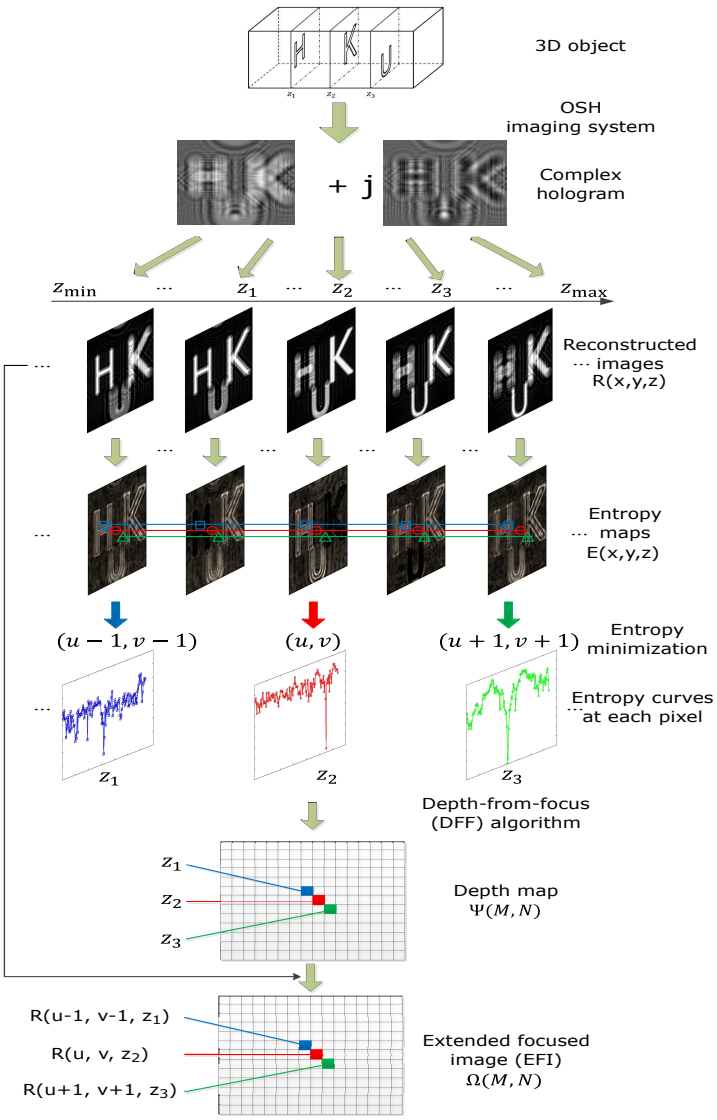

Fig. 4. Computational procedure of our proposed EFI approach. j is the imaginary unit.

The next step is to compute the depth map $\Psi(M, N)$, which is a 2D matrix. As mentioned above, entropy is used as focus measure to determine the best in-focus position. For any pixel (u, v), we can find the minimum entropy value among $E(u, v, z_1)$, $E(u, v, z_2), \ldots, E(u, v, z_k)$. Supposing the minimum entropy occurs at z_i, then we store z_i in Ψ as an index at pixel (u, v). This procedure can be presented as

$$\begin{aligned} \Psi(u, v) &= z_i \\ &= \arg\min_{z \in [z_1, z_k]} E(u, v, z). \end{aligned} \tag{4}$$

The depth map $\Psi(M, N)$ is a 2D matrix storing best in-focus reconstruction distances in $[z_1, z_k]$ at each pixel position. With this depth map Ψ and the volume of reconstructions $R(x, y, z)$, we are able to find the best in-focus pixel value at (u, v) with

$$\begin{aligned} \Omega(u, v) &= R(u, v, z_i) \\ &= R(u, v, \Psi(u, v)), \end{aligned} \tag{5}$$

where Ω denotes the EFI image, which is a 2D matrix with a size of $M \times N$. For other pixels, Eq. 5 is executed in the same way. The overall computational procedure is illustrated in Fig. 4.

IV. Simulation Results

In our simulation, we test our approach on objects with two or three dominant sections respectively. The hologram has a size of 512×512, with a block size chosen to be 21×21. In two-section case, two letters are located at 10 mm ("H") and 20 mm ("K"), while in three-section case, three letters are located at 10 mm ("H"), 15 mm ("K"), and 20 mm ("U"). The reconstruction scanning range is from 8 mm to 22 mm, divided into 128 steps. Thus the scanning step is about 0.11 mm. The smaller the scanning step is, the more reconstructed images we will acquire, and the more precise best in-focus position we can obtain. However, the computation efficiency will decrease drastically. For the block size, larger size will be helpful for estimating the general shape of the object with lower error, but the finer object details are lost.

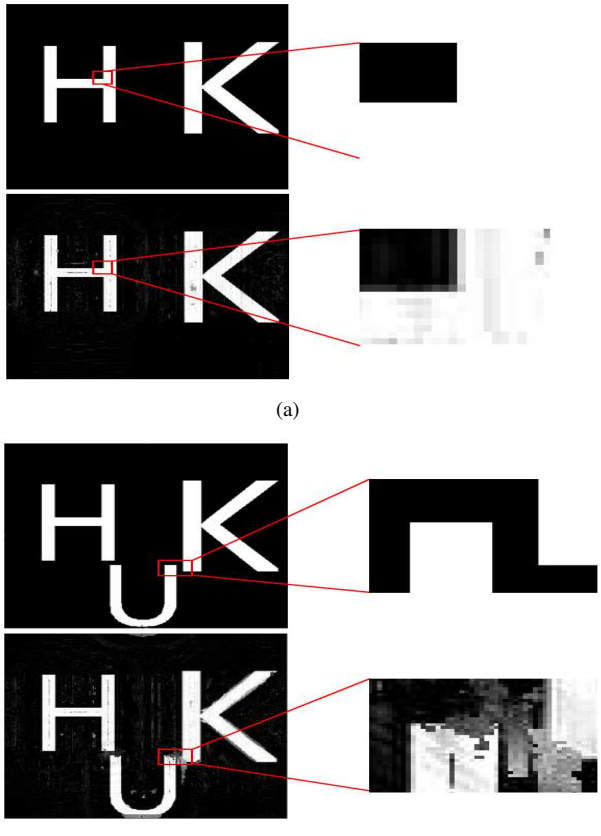

(a)

(b)

Fig. 5. (a) Above: the projection of 3D object composing of two sections (left), and local magnification (right); bottom: the EFI image constructed with our proposed approach (left), and local magnification (right). (b) Above: the projection of 3D object composing of three sections (left), and local magnification (right); bottom: the EFI image constructed with our proposed approach (left), and local magnification (right).

Fig. 5 presents the simulation results on two-section and three-section cases. From the comparison of left parts in Fig. 5(a) and 5(b) we can see that all sections of the 3D object are clear and sharp. All the useful information appears in one single image. Although some noises partially contaminate the EFI image, as figures on the right-hand side in Fig. 5 present. However, the minimal artifacts do not influence the extension of depth-of-field. The final all-in-focus EFI image enables us to be more flexible to analyze and visualize the recorded 3D object.

V. Conclusion

In this paper we propose an approach for constructing EFI based on focus detection with entropy minimization in a holographic microscopy imaging system. Intrinsically the whole 3D information of an object is contained in the digital hologram. In this presented technique we employ this feature to construct one single image where all parts of the recorded 3D object are in-focus. This method constructs the EFI image only by one single hologram, avoiding extra optical components in the experimental setup, as well as the time-consuming mechanical scanning at different focal planes in the recording. The final EFI images in which multiple sections of the two 3D objects are clear and sharp show the extension of DOF. This approach will facilitate the visualization and measurement for microscopic objects in holographic microscopy imaging system. As we can see in Fig. 5, there is still noise contaminating the reconstructed EFI image. This is due to the size of block we are using to filter out specific amount of pixels. Different block size leads to different noise level, as well as the time for computing. In the future, we will try to find an appropriate block size to balance the trade-off between noise level and computation time. Furthermore, how the distances between each section affects the EFI image is also worth investigating.

Acknowledgment

This work was supported in part by the Hong Kong Research Grants Council under Project HKU 7131/12E, and by the NSFC/RGC under N_HKU714/13.

References

[1] D. Gabor, "A new microscopic principle," *Nature*, vol. 161, pp. 777–778, May 1948.

[2] T.-C. Poon, "Scanning holography and two-dimensional image processing by acousto-optic two-pupil synthesis," *Journal of the Optical Society of America A*, vol. 2, pp. 521–527, Apr 1985.

[3] B. W. Schilling, T.-C. Poon, G. Indebetouw, B. Storrie, K. Shinoda, Y. Suzuki, and M. H. Wu, "Three-dimensional holographic fluorescence microscopy," *Optics Letters*, vol. 22, pp. 1506–1508, Oct 1997.

[4] J. Swoger, M. Martinez-Corral, J. Huisken, and E. H. K. Stelzer, "Optical scanning holography as a technique for high-resolution three-dimensional biological microscopy," *Journal of the Optical Society of America A*, vol. 19, pp. 1910–1918, Sep 2002.

[5] T. Kim, "Optical sectioning by optical scanning holography and a Wiener filter," *Applied Optics*, vol. 45, pp. 872–879, Feb 2006.

[6] H. Kim, S.-W. Min, B. Lee, and T.-C. Poon, "Optical sectioning for optical scanning holography using phase-space filtering with Wigner distribution functions," *Applied Optics*, vol. 47, pp. D164–D175, Jul 2008.

[7] E. Y. Lam, X. Zhang, H. Vo, T.-C. Poon, and G. Indebetouw, "Three-dimensional microscopy and sectional image reconstruction using optical scanning holography," *Applied Optics*, vol. 48, pp. H113–H119, Dec 2009.

[8] X. Zhang, E. Y. Lam, and T.-C. Poon, "Reconstruction of sectional images in holography using inverse imaging," *Optics Express*, vol. 16, pp. 17 215–17 226, Oct 2008.

[9] X. Zhang and E. Y. Lam, "Edge-preserving sectional image reconstruction in optical scanning holography," *Journal of the Optical Society of America A*, vol. 27, pp. 1630–1637, Jul 2010.

[10] E. R. Dowski and W. T. Cathey, "Extended depth of field through wavefront coding," *Applied Optics*, vol. 34, pp. 1859–1866, Apr 1995.

[11] D. L. Marks, R. A. Stack, D. J. Brady, and J. van der Gracht, "Three-dimensional tomography using a cubic-phase plate extended depth-of-field system," *Optics Letters*, vol. 24, pp. 253–255, Feb 1999.

[12] V. N. Le, Z. G. Fan, and Q. D. Duong, "To extend the depth of field by using the asymmetrical phase mask and its conjugation phase mask in wavefront coding imaging systems," *Applied Optics*, vol. 54, pp. 3630–3634, Apr 2015.

[13] G. Hausler, "A method to increase the depth of focus by two step image processing," *Optics Communications*, vol. 6, pp. 38–42, Aug 1972.

[14] X. Lin, J. L. Suo, G. Wetzstein, Q. H. Dai, and R. Raskar, "Coded focal stack photography," *IEEE International Conference on Computational Photography*, pp. 1–9, Apr 2013.

[15] P. Ferraro, S. Grilli, D. Alfieri, S. D. Nicola, A. Finizio, G. Pierattini, B. Javidi, G. Coppola, and V. Striano, "Extended focused image in microscopy by digital holography," *Optics Express*, vol. 13, pp. 6738–6749, Sep 2005.

[16] Z. Zalevsky, "Extended depth of focus imaging: a review," *Journal of Photonics for Energy*, p. 018001, Jan 2010.

[17] M. Matrecano, M. Paturzo, and P. Ferraro, "Extended focus imaging in digital holographic microscopy: a review," *Optical Engineering*, vol. 53, p. 112317, Nov 2014.

[18] A. Levin, S. W. Hasinoff, P. Green, F. Durand, and W. T. Freeman, "4D frequency analysis of computational cameras for depth of field extension," *ACM Transactions on Graphics*, vol. 28, pp. 97:1–97:14, Aug 2009.

[19] A. Levin, R. Fergus, F. Durand, and W. T. Freeman, "Image and depth from a conventional camera with a coded aperture," *ACM Transactions on Graphics*, vol. 26, pp. 70:1–70:9, Jul 2007.

[20] A. Agarwala, M. Dontcheva, M. Agrawala, S. Drucker, A. Colburn, B. Curless, D. Salesin, and M. Cohen, "Interactive digital photomontage," *Acm Transactions on Graphics*, vol. 23, pp. 294–302, Aug 2004.

[21] H. J. Zhao, Z. Shang, Y. Y. Tang, and B. Fang, "Multi-focus image fusion based on the neighbor distance," *Pattern Recognition*, vol. 46, pp. 1002–1011, Sep 2013.

[22] M. Antkowiak, N. Callens, C. Yourassowsky, and F. Dubois, "Extended focused imaging of a microparticle field with digital holographic microscopy," *Optics Letters*, vol. 33, pp. 1626–1628, Jul 2008.

[23] C. P. McElhinney, B. M. Hennelly, and T. J. Naughton, "Extended focused imaging for digital holograms of macroscopic three-dimensional objects," *Applied Optics*, vol. 47, pp. D71–D79, Jul 2008.

[24] C. P. McElhinney, J. B. McDonald, A. Castro, Y. Frauel, B. Javidi, and T. J. Naughton, "Depth-independent segmentation of macroscopic three-dimensional objects encoded in single perspectives of digital holograms," *Optics Letters*, vol. 32, pp. 1229–1231, May 2007.

[25] D. Vollath, "Automatic focusing by correlative methods," *Journal of Microscopy*, vol. 147, pp. 279–288, Sep 1987.

[26] X. Zhang, E. Y. Lam, T. Kim, Y. S. Kim, and T.-C. Poon, "Blind sectional image reconstruction for optical scanning holography," *Optics Letters*, vol. 34, pp. 3098–3100, Oct 2009.

[27] M. Liebling and M. Unser, "Autofocus for digital Fresnel holograms by use of a Fresnelet-sparsity criterion," *Journal of the Optical Society of America A*, vol. 21, pp. 2424–2430, Dec 2004.

[28] W. C. Li, N. C. Loomis, Q. Hu, and C. S. Davis, "Focus detection from digital in-line holograms based on spectral ℓ_1 norms," *Journal of the Optical Society of America A*, vol. 24, pp. 3054–3062, Oct 2007.

[29] T. Kim and T.-C. Poon, "Autofocusing in optical scanning holography," *Applied Optics*, vol. 48, pp. H153–H159, Dec 2009.

[30] C. Y. Zhou and S. K. Nayar, "Computational cameras: convergence of optics and processing," *IEEE Transactions on Image Processing*, vol. 20, pp. 3322–3340, Dec 2011.

[31] G. Surya and M. Subbarao, "Depth from defocus by changing camera aperture: a spatial domain approach," *IEEE Conference on Computer Vision and Pattern Recognition*, pp. 61–67, Jun 1993.

[32] C.-K. Liang, T.-H. Lin, B.-Y. Wong, C. Liu, and H. H. Chen, "Programmable aperture photography: multiplexed light field acquisition," *ACM Transactions on Graphics*, vol. 27, pp. 55:1–55:10, Aug 2008.

[33] A. Torralba and A. Oliva, "Depth estimation from image structure," *IEEE Transactions on Pattern Analysis and Machine Intelligence*, vol. 24, pp. 1226–1238, Sep 2002.

[34] S.-H. Lai, C.-W. Fu, and S. Chang, "A generalized depth estimation algorithm with a single image," *IEEE Transactions on Pattern Analysis and Machine Intelligence*, vol. 14, pp. 405–411, Apr 1992.

[35] A. Saxena, S. H. Chung, and A. Y. Ng, "3-D depth reconstruction from a single still image," *International Journal of Computer Vision*, vol. 76, pp. 53–69, Aug 2007.

[36] L. Xi, L. Guosui, and J. Ni, "Autofocusing of ISAR images based on entropy minimization," *IEEE Transactions on Aerospace and Electronic Systems*, vol. 35, pp. 1240–1252, Oct 1999.